Development of a Wearable System to Identify Movement Intentions by Combining Strain Gauges and Inertial Measurement Units

Steve Regis Koalaga, Maxime Raison, Sofiane Achiche

***Abstract*— The combination between surface electromyography sensors and inertial measurement units is the most common multimodal sensing method used in body area networks. Nowadays, this combination is frequently used to identify the intentions of movement in humans, e.g. to control their prosthesis. However, the surface electromyography sensors are usually bulky, with electrodes placed on skin sites, and require a high sampling frequency, usually 1000 Hz, which technically highly reduces the number of sensors that can be used simultaneously by an onboard microprocessor. Further, the electromyographic measurement suffers from crosstalk due to muscles packed side by side. These limitations in electromyography motivates the search for alternatives using multiple sensors capable of operating at lower frequencies for everyday applications at an affordable cost. The objective of this study is to develop a novel wearable system to identify intentions of movement by combining strain gauges and inertial measurement units. The system is composed of 1. two bracelets using six strain gauges each, connected to a flexible printed circuit board and 2. two inertial measurement units. Physiologically, the strain gauges measure the skin deformation due to muscle contraction, while the inertial measurement units provide complementary data on joint kinematics. The system was tested at the upper limb, and successfully identified 9 main movements based on the signal intensity of strain gauges. These results show the great potential of such sensory system to become a smart wearable sensory system to detect human movement intention.**

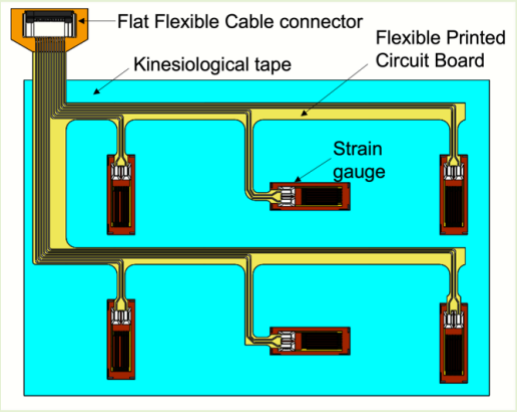

***Index Terms*— strain gauges, IMUs, sensor fusion, movement intention, kinesiological tape.**

I. Introduction

A. On the combination of sEMG-IMU to identify movement intention: context and physiological justification:

THE combination between surface electromyography (sEMG) sensors and inertial measurement units (IMU) is the most common used multimodal sensing method in body area networks [1].Nowadays, this combination is frequently utilized to identify the intention of movement in humans, e.g. for hand and finger gesture recognition [2], or to classify upper limb phantom movements in transhumeral amputees to control their prosthesis (e.g. [3], [4]). And the methods for identification of the intention of movement based on sEMG and IMU have the potential to be extended to daily general applications, such as human computer interfacing [5] [6], teleoperation of industrial robots [7], etc.

The combination between sEMG and IMU can be physiologically justified as a potentially successful avenue, because:

1) sEMG enable to detect the intention of movement, by measuring the muscle activity. Therefore, sEMG is still the main sensor used to control myoelectric prostheses.
2) IMUs provide additional kinematics information about the motion, i.e., articulation configurations, velocities, and accelerations. IMUs fills two limitations of sEMG:
   A. sEMG commonly suffers from the limb position effect, where sEMG signals for the same motion are different in different limb positions [8], [9]. Therefore, IMUs can be complementary.
   B. IMUs are particularly good for capturing larger motions, while sEMG data are better at distinguishing different hand shapes and finger movements [2].

Adding kinematics feature enabled to increase the accuracy of

S.R. Koalaga is with the Mechanical Engineering Department, Polytechnique de Montréal, Montreal QC H3T 1J4, Canada, and also with MARIE ENFANT Rehabilitation Centre, CHU Sainte-Justine, Montreal, QC H1T 1C9, Canada
(e-mail: steve-regis.koalaga@polymtl.ca).
M. Raison is with the Mechanical Engineering Department, Polytechnique de Montréal, Montreal, QC H3T 1J4, Canada, and also with the Rehabilitation Center, Centre hospitalier universitaire Sainte-Justine, Montréal, QC H3T 1C5, Canada
(e-mail: maxime.raison@polymtl.ca).
S. Achiche is with the Mechanical Engineering Department, École Polytechnique de Montréal, Montreal, QC H3T 1J4, Canada
(e-mail: sofiane.achiche@polymtl.ca).

the movement classification by 4.8% [3] on human upper limb movements. Furthermore, Geng *et al.* [10] and Fougner *et al.* [11] presented a classifier in cascades, which reduced the average movement classification error from 18% to 5.7%. This classifier used accelerometry to determine the best limb position before choosing the sEMG classifier [11].

B. Limitations of sEMG and search for alternative solutions

sEMG is a technique that uses electrodes placed on the skin at a specific location to monitor muscle contractions [12]. There are several drawbacks to using sEMG [12], [13]. sEMG can often be unstable due to sweat, electrode shifts, motion artifacts, and electronic noise [12], [14]. Also, crosstalk can occur due to the high number of muscles packed side by side, and muscular fatigue can crucially affect the quality of the signals [12], [14]. Further, the amount of data coming from sEMG, due to the acquisitions generally at 1000 Hz, requires high computing power to process it in real time [15]. Hence, researchers need to pay attention to these critical issues.

Different sensors have been proposed as alternative solutions to using sEMG. Indeed, the growing interest in smart wearable technologies requires the development of new sensors at low cost, with high sensitivity and low detection limit [16]. Liang Zou *et al.* [17] grouped together all tactile sensing systems in four groups, which are capacitive, piezoresistive, piezoelectric and optical tactile sensors. The tactile sensing systems are mostly used in robotics and biomedical engineering. A more detailed work done by [18], introduced *sensor skins* defined to be stretchable planar structures with embedded sensing components. Sensor skin found in the literature can be grouped by the type of material (elastomers, woven fabric), the type of conductor (thin metal films, liquid metal), and the structure they use (microchannels, mechanical flexible interfaces). Chang *et al.* [19] proposed a strain sensor that can still form conformal contact to the skin even during body movements. They are prepared by solution coating and consist of two layers, a dry adhesive layer of biocompatible water-based elastomeric polyurethane, and a detection layer of a non-adhesive composite of reduced graphene oxide and carbon nanotubes. The adhesive layer makes the sensors conform to the skin, while the sensing layer has sensitive resistance to deformations. *Song et al.* [20] presented a strain sensor based on silk graphene spandex coated fabric (GCSS) prepared by reducing graphene oxide. The sensor worked thanks to the extension of the conductive fiber and the deformation of the woven structure. GCSS was successfully used to detect human movement, by providing data for gesture recognition based on deep learning. Yao *et al.* [21] described the application of capacitive strain sensors based on silver nanowires for kinematic finger tracking. The sensors can be attached to the skin to track the movement of the finger joints with minimal interference with daily activities. Ali *et al.* [22], presented a new goniometric glove using flex sensors to capture the user hand gesture that can be used to wirelessly control a bionic hand. However, many of these sensors used a complex fabrication procedure and/or special materials graphene spandex coated fabric, liquid gallium, etc. [17],[18], and were limited to finger movements tracking [19], [20], hence reducing the number of upper limb movements that could be detected in real applications.

C. Strain gauges as the promising solution

Mori *et al.* [23] presented a new bioinstrumentation sensor using one stain gauge for upper limb amputees. Their work concluded that the repeatability of the strain gauge signal is superior to myoelectric signal because the sensor measures the deformation of the skin [23].

Finally, Zizoua *et al.* [15] presented a proof of concept of a bracelet using strain gauges for the identification of four upper limb movements in traumatic amputees: elbow flexion/extension and forearm pronation/supination. Strain gauges can measure small deformation of about 10-13µm and are widely used for their low cost and simple signal conditioning [15].

Therefore, Zizoua *et al.* [15] could be a starting reference as an alternative to EMGs, but this system cannot be used as proposed to identify three-dimensional movements, because of four major limitations:

1) Uniaxial skin deformations: the gauges were placed only in the longitudinal direction of the *biceps brachii* muscle, which does not enable to record multi-axial skin deformations.

2) Fragility: the strain gauges were connected by two thin wires. This enabled a first proof of concept, but was not viable as it either broke or unsoldered when used several times [15].

3) Non-portability: the system was neither compact nor portable, which limits its application in everyday life.

4) Lack of conform contact to skin during movement: the strain gauges were embedded in silicone that did not provide a direct contact with the skin, thus limiting the ability of the system to measure the actual skin deformation.

D. Problem, objective, and research hypotheses

Here above, the state-of-art survey revealed two major problems:

1. The common issues with sEMG were solved by a first proof of concept of bracelet using strain gauges. But this one still had limitations: uniaxial skin deformations, fragility, inaccuracy, and non-portability.
2. The combination between strain gauges and IMUs has never been investigated to detect human motion intention.

Consequently, the objective of this study is to develop a wearable system to identify intentions of movement by combining strain gauges and inertial measurement units.

The main design requirements (DR) of this system are as follows:

DR 1: The system must be able to measure multi-axial skin deformations.

DR 2: The system must be able to be used several times in daily three-dimensional movements.

DR 3: The system must be wearable.

The following research hypothesis (RH) to study can be formulated: “The combination between strain gauges and IMUs could enhance the ability to detect motion intention”.

II. METHODS

The muscle contractions during a movement create a deformation of the skin at the surface. Hence, identifying the muscles involved in the upper limb movement can help to determine the best sites to measure skin deformations and to design the strain gauge bracelet accordingly.

A. Design of a strain gauge bracelet

The strain gauge bracelet consisted of six equally spaced (3.5 cm) strain gauges. These gauges were connected by a 0.1 mm thick flexible printed circuit board (PCB) (see Fig. 1 (a)). In this flexible PCB, the strain gauges with odd numbers (1, 3 and 5) were aligned parallel to the longitudinal direction of the *biceps brachii,* and the strain gauges with even numbers (2, 4, and 6) were aligned perpendicularly to the longitudinal direction of the *biceps brachii*. This configuration enabled to record the skin deformations along two different axes.

The gauges were also able to bend in two directions providing positive (convex deformation) or negative (concave deformation) voltage variation.

The flexible PCB had a 12-position flat flexible connector (FFC). This connector was used to connect the strain gauge bracelet to the acquisition board. The flexible PCB provided a solid connection with the strain gauges.

Different tests were performed with different types and sizes of strain gauges. The tests consisted in applying a deformation to the strain gauges and measuring the signal intensity. The gauge with the best linear response and high intensity was chosen, namely the CF120-10AA. The gauge had a linear pattern and a nominal resistance of 120 ohm ± 1% with a gage factor of 2± 1%. The gauge was made of constantan alloy and had a sensitive grid of 10.0 x 4.0 mm. It was able to measure small strains of about ± 5% of the neutral length which was adequate for our application.

For a better measurement of skin deformation, the gauges, previously soldered on the flexible PCB, were placed directly on a kinesiological tape (see Fig. 1 (b)).

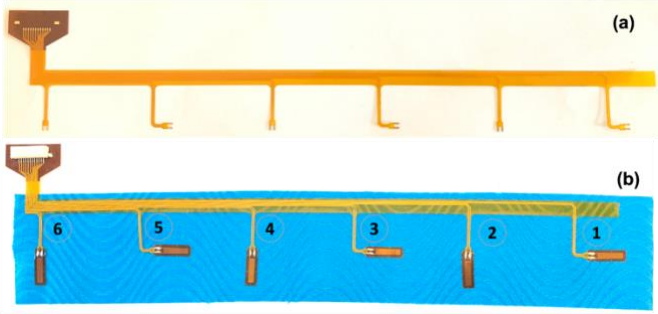

Fig. 1 Strain gauge bracelet. (a) Flexible PCB (yellow) with the connections for 6 strain gauges. (b) Instrumented kinesiological tape (blue) the flexible PCB (yellow) connected to the 6 numbered strain gauges (orange rectangles).

The kinesiological tape was designed to mimic the skin elastic so you can use your full range of motion [24]. The tape used a medical-grade adhesive, which was water-resistant and strong enough to stay on for several days even, while working out or taking showers [25]. Kinesiological tapes are known as therapeutic tape that stretched and, strategically applied to the body to provide support, lessen pain, reduce swelling, and improve performance [26]. A therapist can let you know how much stretch is needed for your treatment. In this study, no stretch was applied to the kinesiological tape, as it was only used as a bonding interface between the strain gauges matrix and the skin. This configuration provided better contact with the skin.

B. The Muscles Involved in Upper Limb Movement

As a proof of concept, one healthy adult subject (male, age: 25 years old, size: 1m70) participated to this study. The experimental procedure was approved by the *Ethic Board* of the *Research Center of Ste-Justine University Hospital Center*, in Montreal. The participant provided informed consent before the experiment and declared being in a good health.

Fig. 2 shows the placement of two bracelets, totalizing 12 strain gauges:

1. Strain gauge bracelet labeled *B* placed around the arm at the *biceps brachii* prominence.
2. Strain gauge bracelet labeled *AB* placed around the forearm 5 cm below the *elbow joint center*; on the forearm and arm.

In this paper, a strain gauge on a bracelet is identified by the label of the bracelet, i.e., *B* or *AB*, followed by the gauge number from 1 to 6 identified in Fig 1 (b). e.g.: The gauge *B6* referrers to strain gauge number 6 on bracelet *B*.

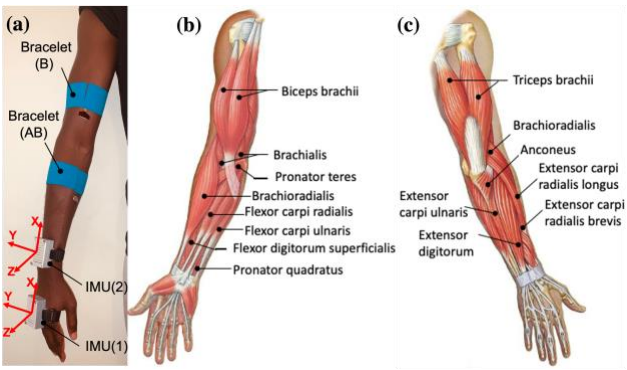

Fig. 2 (a) Placement of the two strain gauge bracelets: bracelet *B* around the arm, and bracelet *AB* placed around the forearm; two IMUS: IMU (1) placed on the hand; IMU (2) placed on the forearm. (b) Anterior view of the human upper limb. (c) Posterior view of the human upper limb. The image (b) and (c) were adapted from [27].

In this study, 10 movements of the upper limb (Fig. 3) were selected. And the muscles responsible for these movements were identified in Table I.

The *biceps brachii*, *brachialis*, and *brachioradialis* muscles are responsible for flexing the forearm. The *triceps brachii* and *anconeus* muscles are responsible for extending the forearm. The gauge *B6* was placed on the center on the *biceps brachii* of the right arm, and the other gauges of strain gauge bracelet *B* were placed going round the arm (X axe of Fig. 2) following the positive direction of the right-hand rule (*B6, B5, B4, B3, B2, B1*).

A *supinator* is a muscle responsible for rotating the forearm so that the palm is facing up or forward. A *pronator* is a muscle that rotates the arm so that the palm is facing down or toward the back. The *extrinsic muscles* of the forearm allow movement of the wrist and hand. The muscles of the *posterior group*

extend the hand to the level of the wrist; the muscles of the *anterior group* flex the hand at the wrist

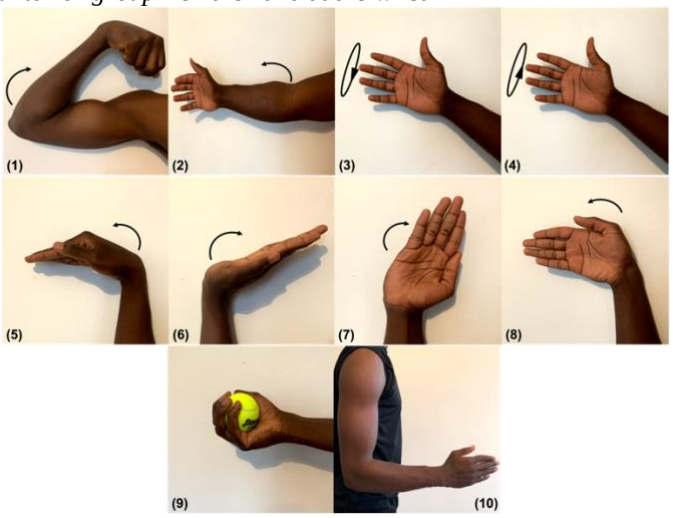

Fig. 3 The 10 identified movements. (1) Elbow Flexion (EF). (2) Elbow Extension (EE). (3) Forearm Pronation (FP). (4) Forearm Supination (FS). (5) Wrist Flexion (WF). (6) Wrist Extension (WE). (7) Wrist Ulnar Deviation (WL). (8) Wrist Radial Deviation (WR). (9) Power grips (PG). (10). Rest position "no movement" (NM).

. The gauge *AB6* was vertically aligned with B6, and the other gauges of strain gauge bracelet *AB* were placed going round the forearm (X axe of Fig. 2) following the positive direction of the right-hand rule (*AB6, AB5, AB4, AB3, AB2, AB1*). The letters *AB* were used to identify this bracelet

Table I identifies the muscles involved in each movement and the main sensors that were placed to capture the movements.

Table I
MUSCLES INVOLVED IN IDENTIFIED UPPER LIMB MOVEMENT.

		Main muscles involved	Main sensors
Elbow movements	EF	-Biceps brachii -Triceps brachii -Brachioradialis -Brachialis	-strain gauge bracelet (B) -IMU (2)
	EE	-Triceps brachii -Biceps brachii -Anconeus	
Forearm movements	FP	-Pronator teres -Pronator quadratus -Supinator -Biceps brachii	-strain gauge bracelet (AB) -IMU (1)
	FS	-Supinator -Pronator Teres -Pronator quadratus	
Wrist movements	WF	-Flexor carpi radialis -Flexor carpi ulnaris -Flexor digitorum superficialis	-strain gauge bracelet (AB) -IMU (1)
	WE	-Extensor carpi radialis longus -Extensor carpi radialis brevis -Extensor digitorum -Extensor carpi ulnaris	
	WL	-Extensor carpi ulnaris	
	WR	-Abducto Polilicis longus -Flexor carpi radialis -Extensor carpi radialis longus -Extensor carpi radialis brevis	
Hand movements	PG	- extrinsic muscles of hand	-strain gauge bracelet (AB)

III. CIRCUITS AND SYSTEM

For each stain gauge bracelet, six analog channels were necessary to record the deformation of the six strain gauges in real time. For inertial unit-based sensors, six signals were acquired, namely tree linear accelerations and tree angular velocities. All sensors had wireless communication.

A. Microcontroller

The microcontroller used for this project was the ESP32. It has a built-in USB-to-serial converter, lithium ion / polymer charger, and pretty much all GPIO outputs. In addition, it enables UART (Universal Asynchronous Receiver-Transmitter), SPI (Serial Peripheral Interface), and I2C communications. The UART protocol was used to establish a communication between the microcontroller and the computer. The computer ran a software to save and visualize the incoming data. The ESP32 has a 240 MHz dual core processor and an Integrated 520 KB SRAM which can perform the heavy calculations for onboard real time movement identification. The I2C protocol was used to connect the microcontroller to the BNO055 IMU.

The ESP32 supports both WiFi and Bluetooth (Classic / LE), this means it is suitable to use for wireless projects. It comes with a proprietary communication protocol ESP-NOW which enables 2-way wireless communication between several ESP32 boards. This protocol was used as it was easy to implement and the transmission's speed was fast enough for our application (>100 Hz).

B. IMU sensor design

The system used a low-cost commercial sensor (BNO055) including an accelerometer, gyroscope, and magnetometer. Fig. 4 shows the wiring diagram.

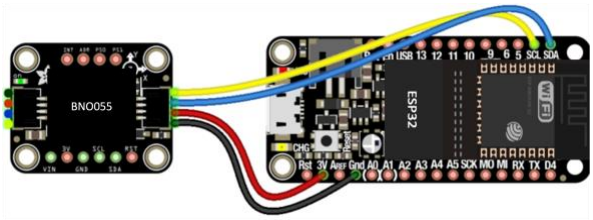

Fig. 3 IMU circuit. BNO055 at left connected to the ESP32 at right using the I2C protocol. The image was adapted from [28].

At first, the BNO055 sensor was connected to the ESP32 using an I2C protocol. It is a serial protocol having a two-wire interface for connecting low speed devices. BNO055 has a 3,3V input which was connected directly into ESP32 3,3Vo. Ground (GND) pin was connected to GND on ESP32, SCL (I2C clock pin) to ESP32 pin 22 and SDA (I2C data pin) to ESP32 pin 23. Following this architecture, two sensors using the BNO055 IMU were implemented.

The code for data acquisition was implemented following the example provided by Adafruit [28]. For each sensor, a BNO055 object was initialized. Each sensor provided linear accelerations and angular velocities along the 3 cartesian axes. A specific identifier was assigned to each sensor as required by the ESP-NOW protocol.

To ensure that the data coming from the BNO055 inertial unit were accurate, it was essential to calibrate the sensors. The calibration was performed according to the calibration guide provided by MathWorks [29]. When the calibration process was completed, the code provided offset values. These offset values were then applied to each axe of the inertial unit.

A 3D printed PLA box was used to hold all electronic devices. The ESP32 has support for connecting a LiPoly / Lion battery. This terminal was connected to a Lipo 850 mAh battery that allowed the system to have an autonomy of 8 hours. A velcro was used to strap the sensor on the arm (see Fig. 7 (b)).

C. Strain gauge-based sensor

After determining the electrical components essential for data acquisition and processing, a PCB (see Fig 6) representing the electrical circuit (see Fig 5) was designed using KICAD open access software.

The PCB had a flat flexible cable connector for connecting the strain gauge bracelet. The PCB included six Wheatstone bridges in quarter bridge configuration. The bridges converted small changes in resistance of the gauges to a voltage. The resistors of this circuit had a nominal resistance value of 120 Ohm with a tolerance of ± 1%. Each bridge had a trimmer potentiometer whose resistance rating is 500 ohms. This potentiometer had twenty turns allowing to have good precision (± 1ohm) which facilitated the bridge zeroing. The zeroing results to a zero-voltage output when no-strain is applied to the gauge. It is an important step to perform before using the system. The signal from the gauges was therefore routed to two multiplexers.

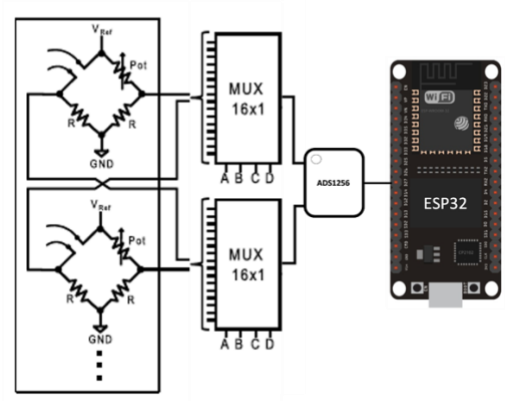

Fig. 4 Electrical circuit for strain gauge signal conditioning showing the Wheatstone bridges in quarter bridge configuration, the multiplexers, the ADS1256 and the ESP32 microcontroller.

The multiplexers allowed to choose the channel to be read by sequentially reading each of the analog inputs. The multiplexer (CD74HC4067) has sixteen channels controlled by 4 digital signals. The data from sixteen strain gauges can be acquired using only one input of a microcontroller. This configuration also allowed the use of a single amplifier and ADC (analog to digital converter). The size of the acquisition system was thus reduced. It also saved equipment costs by using a single amplifier for several gauges.

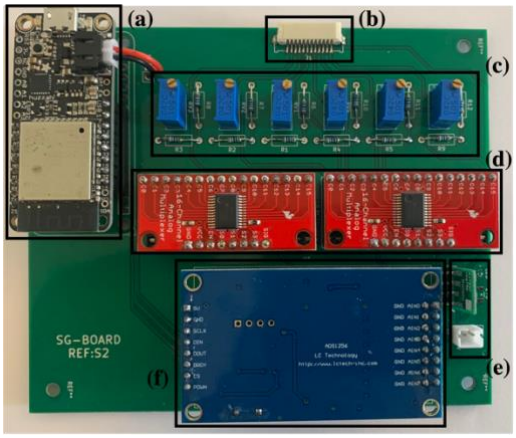

Fig. 5 PCB for strain gauge signal acquisition. (a) ESP32. (b) FFC/FPC connector. (c) Wheatstone Bridge. (d) Multiplexers. (e) Power management. (f) ADS1256.

The analog signals were acquired and processed by the ADS1256. the ADS1256 is a very low noise 24-bit analog-to-digital (A/D) converter. It has a high acquisition frequency of 30 kSPS and can acquire data from 8 asymmetric inputs or 4 differential inputs. The programming of this went through the ESP32 with SPI communication. The ESP32 microcontroller retrieved the data from the ADS1256 in 24-bit digital format. The acquired data were sent to the computer by UART communication. Additionally, a 3,3 V voltage regulator was added to provide a stable voltage source for the Wheatstone's bridges. The stability of the voltage source is important to ensure the stability of Wheatstone bridges.

This acquisition board was powered by a LiPo (Lithium Polymer) battery with a capacity of 5000 mAh at 3,7 V and a power of 18.5 W. This battery allowed the acquisition system to have an autonomy of 24 hours. A 3D printed PLA box was used to hold all electronic devices (see Fig. 7(a)).

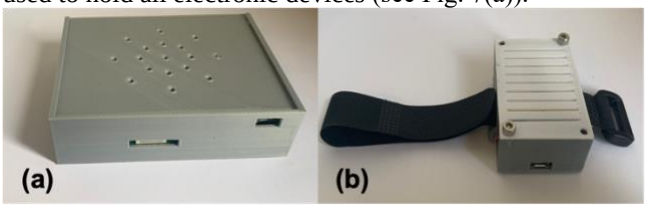

Fig. 6 3D printed box for electronics. (a) Box (12x10x3.3 cm) containing the PCB for strain gauge signal conditioning. (b) Box (5.5x3.5x2.2 cm) containing the IMU circuit and a Velcro strap.

D. Signal Acquisition

The sensors used wireless communication based on the ESP-NOW protocol. The communication architecture is presented in Fig. 8. A total of 12 signals from the strain gauges were recorded for each movement. In addition to these signals, the triaxial linear accelerations and angular velocities coming from two IMUs were used. Combining the signals from the strain gauges and inertial units, a total of 24 signals were obtained. The data were sampled at a frequency of 100 Hz. The frequency of 100 Hz was chosen to limit the amount of data to be processed. Human movement frequency is 0-20 Hz [30]; hence the theorem of Shannon Nyquist was respected. A Butterworth-

type digital low-pass filter of order 4 with a cut-off frequency of 1 Hz was used to filter the signal from the strain gauges. The first hundred data for each gauge was averaged and used to set an offset for the following data. The raw signals from IMUs were used.

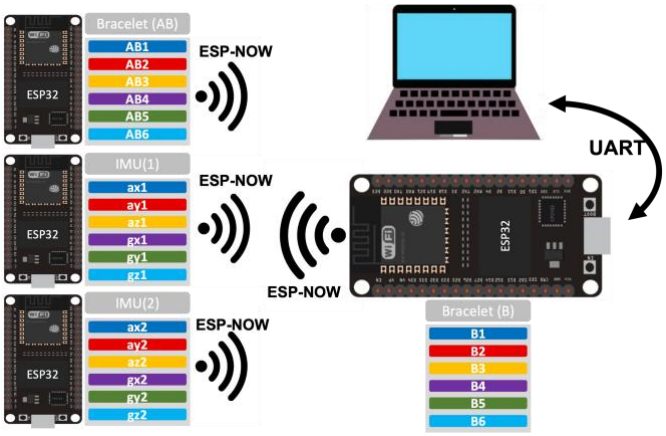

Fig. 7 Communication architecture including the microcontroller, the communication protocols (ESP-NOW, UART), and the variables corresponding to the sensors output.

IV. Results

A sequence of movements was established to verify the system. The sequence was as follows *EF-NM-EE-NM-FP-NM-FS-NM-WF-NM-WE-NM-WL-NM-WR-NM-PG-NM*. The resting position *NM* was observed between each movement.

Fig. 9 shows the data acquired during the sequence of movement performed by the subject. Fig 9 (a) shows the 3 linear accelerations and 3 angular velocities coming from IMU (1) which was placed on the hand. Fig 9 (b) shows the 3 linear accelerations and 3 angular velocities coming from IMU (2) which was placed on the forearm. Fig 9 (c) shows the data acquired by the strain gauge bracelet placed on the arm. Fig 9 (d) shows the data acquired by the strain gauge bracelet placed on the forearm.

In Table I, the maximum voltage variation for each strain gauge was computed per movement. The gauges that have recorded a voltage variation (ΔV) superior to 1 mV were identified.

Furthermore, using the information in Table II the maximum ΔV in both bending directions were computed per column to determine which strain gauges recorded more skin deformation for a particular movement, and per row to determine which movement produced the maximum ΔV for each gauge. The results are displayed in Table III and described here below.

1) Elbow Flexion (EF): The strain gauges that recorded larger deformations were *B6*, *AB6* and *AB1*, with 4.5 mV, 6.03 mV, and 4.48 mV, respectively. Compared to all strain gauges, *AB6*, *AB3* recorded the greatest deformations for this movement in both bending directions. Compared to other movements, strain gauges *B6*, *AB1*, *AB6* recorded their greatest convex deformation and *B3* recorded its greatest concave deformation. IMU (1) and IMU (2) recorded similar angular velocities (*gz1*, *gz2*) around the Z-axis

2) Elbow Extension (EE): The strain gauges that recorded larger deformations were *B1*, *B5*, *B6* with -4.11mV, -2.99mV and -1.98mV, respectively. Compared to all strain gauges, *AB6*, *AB1* recorded the greatest deformations for this movement in the two bending directions. Compared to other movements, strain gauges *B1*, *B2*, *B5* recorded their greatest concave deformation. IMU (1) and IMU (2) recorded similar angular velocities (*gz1*, *gz2*) around the Z-axis.

3) Forearm Pronation (FP): The strain gauges *B2*, *B4* with 1.67 mV, 1.04 mV, respectively and *AB1* and *AB3* with 1.61 mV, 0.95 mV respectively recorded larger deformations. Compared to all strain gauges, *B2*, *B3* recorded the greatest deformations for this movement in both bending directions. Compared to other movements, strain gauges *B2*, recorded its greatest convex deformation. IMU (1) and IMU (2) recorded similar angular velocities (*gx1*, *gx2*) around the X-axis.

4) Forearm Supination (FS): The strain gauges *AB3*, *AB1*, *AB6*, *AB2*, with -1.66mV, 1.30 mV, -1.14mV, 1.02 mV respectively and *B6* with -1.14mV recorded larger deformations. Compared to all strain gauges, *B6*, *AB3* recorded the greatest deformations for this movement in both bending directions. None of the gauges recorded their maximal deformation during forearm supination. IMU (1) and IMU (2) recorded similar angular velocities (*gx1*, *gx2*) around the X-axis.

5) Wrist Flexion (WF): The strain gauges *AB1*, *AB2 AB5* with 2.41 mV, 1.36 mV, -1.89mV respectively and *B6* with 1.81 mV recorded larger deformations. Compared to all strain gauges, *AB1*, *AB5* recorded the greatest deformations for this movement in both bending directions. Compared to other movements, strain gauges *AB5* recorded its greatest concave deformation

6) Wrist Extension (WE): The strain gauges *B4*, *B6* with 1.34 mv, 1.35 mV, respectively and *AB1*, *AB2*, *AB3*, *AB4* with -3.40mV, 1.55 mV, 1.52 mV, 1.06 mV respectively recorded larger deformations. Compared to all strain gauges, *AB2*, *AB6* recorded the greatest deformations for this movement in both bending directions. Compared to other movements, strain gauges *B4* recorded its greatest convex deformation. IMU (1) recorded angular velocities (*gy1*) around the Y-axis. IMU (2) placed on the forearm did not record any movement.

7) Wrist Ulnar deviation (WL): The strain gauges *B6* with 1.39 mV and *AB1*, *AB2* and *AB3* with 2.65 mV, 1.58 mV, 2.19 mV respectively recorded larger deformations. Compared all strain gauges, *AB1*, *B3* recorded the greatest deformations for this movement in both bending directions. Compared to other movements, strain gauges *B1*, *AB3* recorded their greatest concave deformations. IMU (1) and IMU (2) recorded similar angular velocities (*gz1*, *gz2*) around the Z-axis.

8) Wrist Radial deviation (WR): The strain gauges *B2*, *B6*, with 1.26 mV, 1.02 mV respectively and *AB1*, *AB2*, *AB4*, *AB5*, *AB6* with -4.32mV, 1.67 mV, 1.22 mV and 1.14 mV respectively recorded larger deformations. Compared to all strain gauges, *AB2*, *AB1* recorded the greatest deformations for this movement in both bending directions. Compared to other movements, strain gauges *B5*, *AB4*, *AB5* recorded their greatest convex deformation and *AB1*, *AB6* recorded its greatest concave deformation. IMU (1) and IMU (2) recorded similar angular velocities (*gz1*, *gz2*) around the Z-axis.

9) Power Grips (PG): The strain gauges *AB1*, *AB2*, *AB3* with 1.71 mV, 1.81 mV and -2.32 mV respectively recorded larger

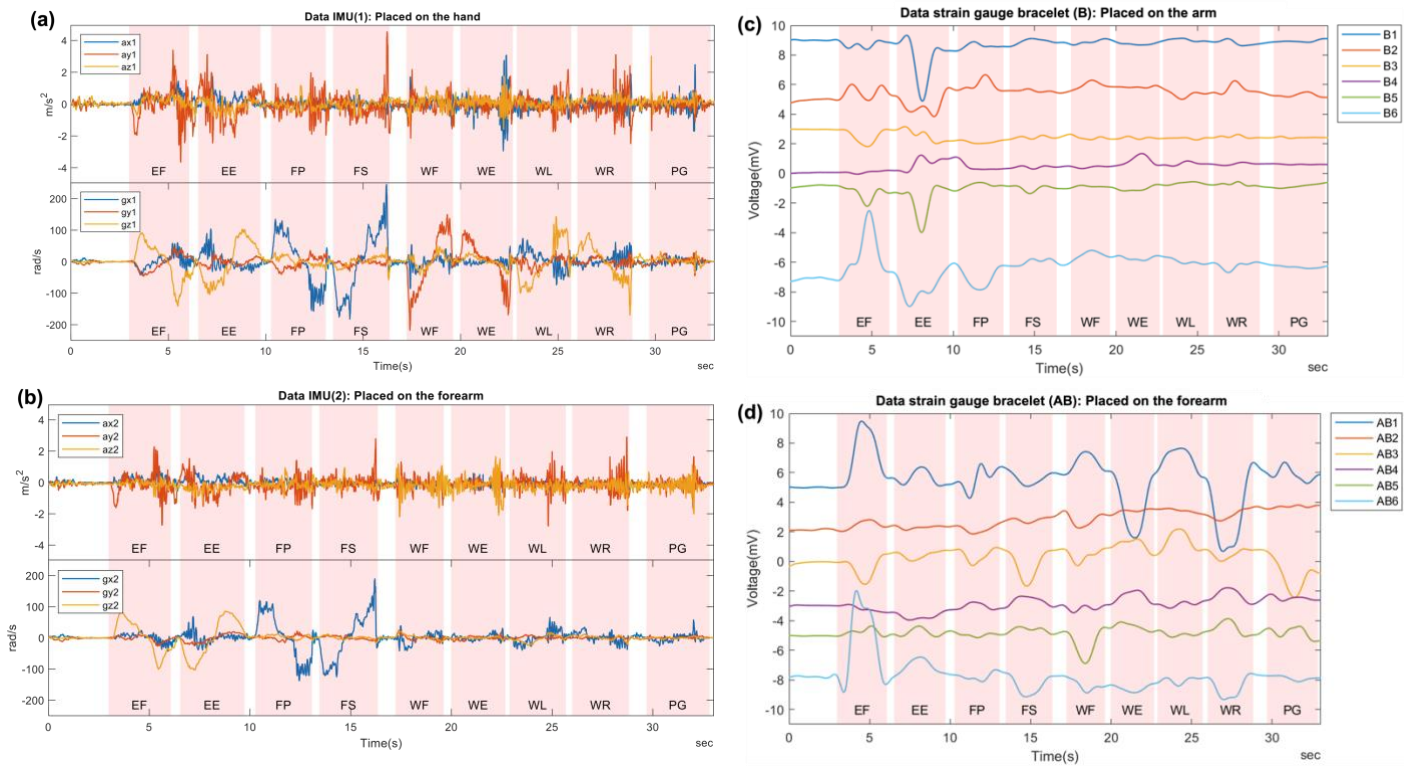

Fig. 8 (a) Tri-axial linear acceleration and triaxial angular velocity from the IMU (1) placed on the hand. (b) Tri-axial linear acceleration and triaxial angular velocity from the IMU (2) placed on the forearm. (c) Data from the six strain gauges in the bracelet placed on the arm (B). (d) Data from the six strain gauges in the bracelet placed on the forearm (AB)

TABLE II.
PEAK SIGNAL INTENSITY FOR EACH STRAIN GAUGE PER MOVEMENT(MV)

	EF	EE	FP	FS	WF	WE	WL	WR	PG
B1	-0.62	**-4,11**	-0.71	-0.43	-0.32	-0.32	0.13	-0.37	-0.14
B2	**1.02**	**-1.15**	**1.67**	0.72	**1.30**	0.94	0.74	**1.26**	0.51
B3	**-1.19**	-0.98	-0.98	-0.70	-0.72	-0.69	-0.74	-0.62	-0.63
B4	0.21	**1.24**	**1.09**	0.52	0.50	**1.34**	0.85	0.76	0.66
B5	**-1.22**	**-2.99**	0.39	-0.36	0.20	0.26	0.44	0.45	0.35
B6	**4.50**	**-1.98**	-0.85	**1.25**	**1.81**	**1.45**	**1.39**	**1.02**	0.80
AB1	**4.48**	**1.38**	**1.61**	**1.30**	**2.41**	**-3.40**	**2.65**	**-4.32**	**1.71**
AB2	0.82	0.44	0.60	**1.01**	**1.36**	**1.55**	**1.58**	**1.67**	**1.81**
AB3	**-1.54**	0.76	**0.95**	**-1.66**	0.89	**1.52**	**2.19**	0.85	**-2.42**
AB4	-0.45	-0.95	-0.26	0.65	-0.46	**1.06**	0.30	**1.22**	0.79
AB5	0.65	0.64	0.24	0.59	**-1.89**	0.91	0.35	**1.14**	0.62
AB6	**6.03**	**1.54**	0.69	**-1.14**	-0.88	-0.86	-0.41	**-1.32**	0.29

TABLE III.
STRAIN GAUGE SIGNAL INTENSITY PATTERN.

	Maximum voltage variation per strain gauge		Maximum voltage variation per movement	
	(+) mV max	(-) mV Min	(+) mV max	(-) mV max
EF	B6, AB1, AB6	B3	AB6	AB3
EE	-	B1, B2, B5, B6, AB4	AB6	AB1
FP	B2	-	B2	B3
FS	-	-	B6	AB3
WF	-	AB5	AB1	AB5
WE	B4	-	AB2	AB6
WL	B1, AB3	-	AB1	B3
WR	B5, AB4, AB5	AB1, AB6	AB2	AB1
PG	AB2	AB3	AB2	AB3

deformations. Compared to all strain gauges, AB2, AB3 recorded the greatest deformations for this movement in both bending directions. Compared to other movements, strain gauges AB2 recorded its greatest convex deformation and AB3 recorded its greatest concave deformation. IMU (1) recorded angular velocities (gy1) around the Y-axis. IMU (2) placed on the forearm didn't record any movement.

V. DISCUSSION

In this work a new generation of sensor combining strain gauges and inertial units was presented to identify intentions of movements of the human upper limb.

A. Movement identification

Table I identifies the muscles responsible for each movement. Fig. 2 shows the placement of the sensors regarding the muscles involved in the upper limb motion. A link was established between the movements performed by the subject (Fig. 3) and the signal recorded by the strain gauges (Fig. 9).

1) Elbow Flexion (EF): The strain gauge *B6* was placed on the *biceps brachii* which explains the high intensity signal (Fig. 9). By going around the arm with the strain gauge bracelet *(AB)*, *AB1* and *AB6* were placed near the *brachioradialis*, which explains the deformation obtained. However, the gauge *B6* was expected to record more deformation as the *biceps brachii* is the main muscle responsible of the flexion of the forearm.

2) Elbow Extension (EE): The *strain* gauges *B1* and *B6* were placed on the *biceps brachii* which relaxes during the elbow extension. It is therefore normal to record deformations in the opposite direction to the bending movement for gauges *B6* and *B1*(Fig. 9(c)). The signal of *B6* went from positive for elbow flexion to negative for elbow extension. The strain gauge *B5* was placed closed to the *Brachialis* which also relaxes during elbow extension. The gauges *AB1* and *AB6* were placed near the *Brachioradialis* and recorded deformations. These measurements can be explained by the nature of the extension movement which tends to stretch the skin of the forearm at full range of motion.

3) Forearm Pronation (FP): The strain gauges *AB1* and *AB3* were placed around the *pronator teres* which is mainly responsible for the pronation of the forearm. It is therefore normal that *AB1* and *AB3* recorded signals with high intensity. The *biceps brachii* is partly involved in the pronation movement of the forearm. The movement of the biceps creates large deformation of the skin around the arm which matches the high intensity signals recorded by strain gauges *B2* and *B4*.

4) Forearm Supination (FS): The strain gauges *AB1*, *AB2* and *AB3* were located around the *supinator* which is responsible for the supine movement of the forearm. The strain gauges *AB1* and *AB3* were involved in both pronation, and supination. *B6* is centered on the *biceps brachii* which is involved in this movement. The forearm pronation and supination movement are like a twisting movement which causes the skin of the forearm to stretch, it is normal that most of the strain gauges of the bracelet placed on the forearm recorded deformations.

Most of the muscles involved in the subsequent movements are in the forearm. Hence, the gauges of the bracelet(B) placed on the arm recorded decreasingly weak signals (Fig. 9 (c)). The muscles in the forearm are packed side by side or overlapped so it was more difficult to make a link between the muscles involved in the movement and the placement of the strain gauges.

5) Wrist Flexion (WF): The strain gauges *AB1*, *AB2*, *AB5* were found close to the muscle group involved in the flexion movement of the wrist. The gauge *AB1* gauge is centered on the *flexor carpi radialis* which explains a stronger signal.

6) Wrist Extension (WE): The strain gauges *AB1*, *AB2*, *AB3*, *AB4* were found near the muscles involved in the extension movement of the wrist. *AB1* is near the *extensor carpi ulnaris*, and the *digitorum extender* which explains a stronger signal.

7) Wrist Ulnar deviation (WL): The muscles responsible for the ulnar deviation of the wrist is the *extensor Carpi ulnaris*. The strain gauges *AB1* and *AB3* were placed near this muscle, which explains the signals recorded.

8) Wrist Radial deviation (WR): The muscles responsible for the radial deviation of the wrist are the *flexor carpi radialis, extensor carpi radialis longus, extensor carpi radialis Brevis*. This group of muscles goes almost all around the forearm, which explains the deformations recorded by most of the gauges of the strain gauge bracelet placed on the forearm.

9) Power Grips (PG): The gripping movement mainly involves the extrinsic and intrinsic muscles of the hand. Certain muscles of the forearm (e.g., *flexor digitorum superficialis*) are involved in power grips which explains the signals recorded by strain gauges *AB1*, *AB2*, and *AB3*.

Data from IMUs (Fig 9 (a), (b)) provided additional information about the motion. Although it was difficult to have a visual interpretation of the linear acceleration's data, the angular velocities provided information used to derive a relation between the graphs obtained and the movements.

For the movements of *EF*, *EE*, *FP* and *FS* it was expected to register similar signals of linear acceleration and angular velocities from the two IMUs. Indeed, for these movements the IMUs were aligned along the same axes and the wrist remained fixed which simulates two IMUs placed on a rigid bar. The observations of the graphs confirmed our assertion.

The movements of *WF*, *WE*, *WR*, *WL* showed a quasi-static angular acceleration for the IMU placed on the forearm (Fig. 9 (b)). Indeed, only the wrist performs these movements, so it is normal to record accelerations only from the IMU (1) placed on the hand. The gripping movement consisted of opening and closing the hand, so no acceleration nor velocities should be recorded by the IMUs. However, humans can hardly maintain a perfect static position, hence the observation of slight accelerations was normal (Fig. 9(a), (b)).

The results showed that the strain gauge bracelet placed on the forearm recorded signals that can distinguish between different wrist movements and the power grips movement. The strain gauge bracelet placed on the arm recorded signals that can distinguish between forearm movements. Also, the combination of strain gauges that recorded maximum ΔV is unique for each movement (see Table III). This uniqueness represents a pattern to identify upper limb movement.

Referring to Table III, it is worth noting that:

1) There was no strain gauge which measured its greatest deformation for *forearm supination*. Hence, no strain gauge was optimally placed to detect *forearm supination*.
2) The strain gauge *AB6* recorded its maximum ΔV and recorded more signal for *elbow flexion* compared to other strain gauges. This strain gauge is a good discriminant for this *elbow flexion*.
3) The strain gauge *B2* recorded its maximum ΔV and recorded more signal for forearm pronation compared to other strain gauges. This strain gauge is a good discriminant for *forearm pronation*.
4) The strain gauge *AB5* recorded its maximum ΔV and recorded more signal for *wrist flexion* compared to other strain gauges. This strain gauge is a good discriminant for *wrist flexion*.
5) The strain gauge *AB1* recorded is maximum ΔV and recorded more signal for *wrist radial deviation* compared to other strain gauges. This strain gauge is a good discriminant for this *wrist radial deviation.*
6) The strain gauges *AB2* and *AB3* recorded their maximum ΔV and recorded more signal for *power grasp* compared to other strain gauges. These gauges are good discriminants for *power grasp*.

The impacts of adding IMUs to the system are as follows:

1) The angular velocities helped to identify the end and beginning of each movement in the sequence.
2) The position of the limb could be inferred using angular velocities.

3) The linear acceleration contribution is unclear at this point. However, further analysis using different techniques could provide more information regarding the kinematics data.

The strain gauges provided information about muscle contraction and the IMUs provided information about the motion. The preliminary results obtained proved the capability of this sensor to record signals making it possible to distinguish 9 movements of the upper [**RH**].

B. Sensor design:

Moreover, the proposed system was compact and portable making ideal for daily activities (Fig. 7 (a), (b)). The strain gauge bracelet used strain gauge and kinesiological tape which are commercially available. The IMU (1) placed on the hand was not optimal regarding its size. However, sensor of smaller size can solve this issue.

Each strain gauge in the matrix collected a specific signal. The third and fourth maximum ΔV (see Table II) were recorded by gauges *B1*(4.48 mV) and *AB1*(-4.11mV) which were placed horizontally (Fig. 1). Aligning the strain gauges in the direction of the greatest strain [15] was not optimal since the sensor did not record the deformation about the other axis. This information can be very useful for a future classification algorithm to distinguish between different movements. Measuring strain on multiple axes is therefore important to better capture skin deformation due to muscle activity [**DR1**].

The new flexible PCB-based strain gauge matrix fabrication method was systematic, so the shape, size and orientation of the gauges can be changed depending on the application. Different strain gauge matrices can be made using flexible PCBs and placed in different sites on the human body to collect different information [**DR3**]. This technique also provided a good solid connection with the gauges that prevented the connections to break or unsolder during movements [**DR2**] as a solution to the robustness issues noted in [15].

The number of strain gauges, their orientations as well as the position of the strain gauge bracelet are important factors that can be optimized by referring to basic knowledge of human anatomy. This knowledge does not need to be specific as it is in the case of sEMG which requires the sensors to be placed on the right muscle to detect the right signal [12]. The system had 12 channels of strain gauges, and more strain gauges can be added if necessary. It is nearly impossible/or too bulky to place the same number of sEMG electrodes on a person without interfering with his daily activities. Also, the frequency of data acquisition of the proposed system was customizable between 40 Hz to 200 Hz which is far less than sEMG sampling frequency (1000 Hz)[14]. A technical limitation related to the use of Wheatstone bridge was the need to recalibrate each bridge after certain amount of use. A subsequent work can investigate that issue.

VI. Conclusion

The objective of this research was to develop a novel wearable system to identify intentions of movement by combining strain gauges and inertial measurement units. The proposed system is composed of 1. two strain gauge bracelets using 6 strain gauges each, connected to a flexible printed circuit board and 2. two inertial measurement units. The system was tested on the upper limb, and successfully identified 9 main movements through the variations in signal intensity of the strain gauges. However, the data collected was rich in information and a machine learning or deep learning algorithm could better capture the underlying patterns of each movement. These results show the potential of such sensory system to become a smart wearable sensory system to detect human movement intention. The future perspectives will be to extend the system, e.g., to the lower limbs, and to identify complex movement combinations by using pattern recognition algorithms with such sensory system.

References

[1] A. Duivenvoorden, K. Lee, M. Raison, and S. Achiche, "Sensor fusion in upper limb area networks: A survey," *2017 Glob. Inf. Infrastruct. Netw. Symp. GIIS 2017*, vol. 2017-Decem, pp. 56–63, 2017, doi: 10.1109/GIIS.2017.8169802.

[2] M. Georgi and T. Schultz, "Recognizing Hand and Finger Gestures with IMU based Motion and EMG based Muscle Activity Sensing," pp. 99–108, 2015.

[3] G. Gaudet, M. Raison, and S. Achiche, "Classification of Upper limb phantom movements in transhumeral amputees using electromyographic and kinematic features," *Eng. Appl. Artif. Intell.*, vol. 68, no. April 2017, pp. 153–164, 2018, doi: 10.1016/j.engappai.2017.10.017.

[4] F. Gaetani, G. A. Zappatore, P. Visconti, and P. Primiceri, "Design of an Arduino-based platform interfaced by Bluetooth low energy with Myo armband for controlling an under-actuated transradial prosthesis," *ICICDT 2018 - Int. Conf. IC Des. Technol. Proc.*, pp. 185–188, 2018, doi: 10.1109/ICICDT.2018.8399787.

[5] U. Muhammad, K. A. Sipra, M. Waqas, S. Tu, and A. Koubaa, "POSTER: Human-Robot Interaction: A Myo Armband Using EMG and IMU Signals," *Proc. - 2020 1st Int. Conf. Smart Syst. Emerg. Technol. SMART-TECH 2020*, pp. 251–252, 2020, doi: 10.1109/SMART-TECH49988.2020.00064.

[6] G. D. Morais, L. C. Neves, A. A. Masiero, and M. C. F. Castro, "Application of Myo Armband System to control a robot interface," *BIOSIGNALS 2016 - 9th Int. Conf. Bio-Inspired Syst. Signal Process. Proceedings; Part 9th Int. Jt. Conf. Biomed. Eng. Syst. Technol. BIOSTEC 2016*, no. January, pp. 227–231, 2016, doi: 10.5220/0005706302270231.

[7] M. Çoban and G. Gelen, "Wireless teleoperation of an industrial robot by using myo arm band," *2018 Int. Conf. Artif. Intell. Data Process. IDAP 2018*, 2019, doi: 10.1109/IDAP.2018.8620789.

[8] R. Gravina, P. Alinia, H. Ghasemzadeh, and G. Fortino, "Multi-sensor fusion in body sensor networks: State-of-the-art and research challenges," *Inf. Fusion*, vol. 35, pp. 68–80, 2017, doi: https://doi.org/10.1016/j.inffus.2016.09.005.

[9] D. Novak and R. Riener, "A survey of sensor fusion methods in wearable robotics," *Rob. Auton. Syst.*, vol. 73, pp. 155–170, 2015, doi: 10.1016/j.robot.2014.08.012.

[10] Y. Geng, P. Zhou, and G. Li, "Toward attenuating the impact of arm positions on electromyography pattern-recognition based motion classification in transradial amputees," *J. Neuroeng. Rehabil.*, vol. 9, no. 1, pp. 1–11, 2012, doi: 10.1186/1743-0003-9-74.

[11] A. Fougner, E. Scheme, A. D. C. Chan, K. Englehart, and Ø. Stavdahl, "Resolving the limb position effect in myoelectric pattern recognition," *IEEE Trans. Neural Syst. Rehabil. Eng.*, vol. 19, no. 6, pp. 644–651, 2011, doi: 10.1109/TNSRE.2011.2163529.

[12] M. B. I. Reaz, M. S. Hussain, and F. Mohd-Yasin, "Techniques of EMG signal analysis: Detection, processing, classification and applications," *Biol. Proced. Online*, vol. 8, no. 1, pp. 11–35, 2006, doi: 10.1251/bpo115.

[13] M. Connan, E. R. Ramírez, B. Vodermayer, and C. Castellini, "Assessment of a wearable forceand electromyography device and comparison of the related signals for myocontrol," *Front. Neurorobot.*, vol. 10, no. NOV, pp. 1–13, 2016, doi: 10.3389/fnbot.2016.00017.

[14] E. Criswell, *Cram's introduction to surface electromyography*. Jones & Bartlett Publishers, 2010.

[15] C. Zizoua, M. Raison, S. Boukhenous, M. Attari, and S. Achiche, "Development of a Bracelet With Strain-Gauge Matrix for Movement Intention Identification in Traumatic Amputees," *IEEE Sens. J.*, vol. 17, no. 8, pp. 2464–2471, 2017, doi: 10.1109/jsen.2017.2666784.

[16] Y. Bu *et al.*, "Ultrasensitive strain sensor based on superhydrophobic microcracked conductive Ti3C2Tx MXene/paper for human-motion monitoring and E-skin," *Sci. Bull.*, vol. 66, no. 18, pp. 1849–1857, 2021, doi: https://doi.org/10.1016/j.scib.2021.04.041.

[17] L. Zou, C. Ge, Z. J. Wang, E. Cretu, and X. Li, "Novel tactile sensor technology and smart tactile sensing systems: A review," *Sensors (Switzerland)*, vol. 17, no. 11, pp. 1–24, 2017, doi: 10.3390/s17112653.

[18] J. A. Rogers, R. Ghaffari, and D.-H. Kim, "Stretchable Bioelectronics for Medical Devices and Systems," *Stretchable Bioelectron. Med. Devices Syst.*, pp. 257–273, 2016, doi: 10.1007/978-3-319-28694-5.

[19] S. Wang, Y. Fang, H. He, L. Zhang, C. Li, and J. Ouyang, "Wearable Stretchable Dry and Self-Adhesive Strain Sensors with Conformal Contact to Skin for High-Quality Motion Monitoring," *Adv. Funct. Mater.*, vol. 31, no. 5, p. 2007495, Jan. 2021, doi: https://doi.org/10.1002/adfm.202007495.

[20] X. Song *et al.*, "A graphene-coated silk-spandex fabric strain sensor for human movement monitoring and recognition," *Nanotechnology*, vol. 32, no. 21, p. 215501, 2021, doi: 10.1088/1361-6528/abe788.

[21] S. Yao, L. Vargas, X. Hu, and Y. Zhu, "A Novel Finger Kinematic Tracking Method Based on Skin-Like Wearable Strain Sensors," *IEEE Sens. J.*, vol. 18, no. 7, pp. 3010–3015, 2018, doi: 10.1109/JSEN.2018.2802421.

[22] S. A. A. Syed Mubarak Ali, N. S. Ahmad, and P. Goh, "Flex sensor compensator via hammerstein–wiener modeling approach for improved dynamic goniometry and constrained control of a bionic hand," *Sensors (Switzerland)*, vol. 19, no. 18, 2019, doi: 10.3390/s19183896.

[23] T. Mori, Y. Tanaka, and M. Mito, "Clinical tests on bioinstrumentation using shape deformation of amputated upper limb," *2013 IEEE/SICE Int. Symp. Syst. Integr. SII 2013*, pp. 505–510, 2013, doi: 10.1109/sii.2013.6776695.

[24] M. Maselli, E. Mussi, F. Cecchi, M. Manti, P. Tropea, and C. Laschi, "A wearable sensing device for monitoring single planes neck movements: Assessment of its performance," *IEEE Sens. J.*, vol. 18, no. 15, pp. 6327–6336, 2018, doi: 10.1109/JSEN.2018.2847454.

[25] S. Wang *et al.*, "Stretchable and wearable triboelectric nanogenerator based on kinesio tape for self-powered human motion sensing," *Nanomaterials*, vol. 8, no. 9, 2018, doi: 10.3390/nano8090657.

[26] D. Morris, D. Jones, H. Ryan, and C. G. Ryan, "The clinical effects of Kinesio® Tex taping: A systematic review," *Physiother. Theory Pract.*, vol. 29, no. 4, pp. 259–270, 2013, doi: 10.3109/09593985.2012.731675.

[27] P. Education, "Chapter 10: The muscular system," 2015. https://www.pearsonhighered.com/assets/samplechapter/0/1/3/4/0134396405.pdf.

[28] A. Kay, "Adafruit 9-DOF Absolute Orientation IMU Fusion Breakout - BNO055 - STEMMA QT / Qwiic." .

[29] MathWorks, "Calibrate BNO055 Sensors." https://www.mathworks.com/help/supportpkg/arduinoio/ug/calibrate-sensors.html.

[30] R. Khusainov, D. Azzi, I. E. Achumba, and S. D. Bersch, "Real-time human ambulation, activity, and physiological monitoring: Taxonomy of issues, techniques, applications, challenges and limitations," *Sensors (Switzerland)*, vol. 13, no. 10, pp. 12852–12902, 2013, doi: 10.3390/s131012852.

Steve Regis Koalaga received a bachelor's in mechanical engineering from Polytechnique Montreal with a minor in robotics and artificial intelligence in 2019. He is currently finalizing a Master's thesis in Applied Science at the *Robotics and Artificial Intelligence Laboratory* (prof. Maxime Raison) and the *Intelligent and Mechatronic Systems Design Laboratory* (prof. Sofiane Achiche) at Polytechnique Montreal, Canada. His research interests include biomedical engineering, electronics, artificial intelligence and mechatronics systems.

Maxime Raison obtained a degree in electrical engineering and a Ph.D. degree in mechanical engineering from *UCLouvain*, Belgium. He is now full professor in mechanical and biomedical engineering at *Polytechnique Montreal*, Canada, where he teaches *Dynamic measurement and modeling*, and *Rehabilitation engineering*. He is the director of the *Robotics and Artificial Intelligence Laboratory* and is affiliated to the *Research Center of Ste-Justine University Hospital Center* in Montreal. His main research topics are multibody dynamic modeling, assistive robotics, and artificial intelligence in biomedical engineering.

Sofiane Achiche received the M.Sc.A. and Ph.D. degrees from *Polytechnique Montreal*, Canada. He is currently a full professor with the *Mechanical Engineering Department*, *Design of Machinery Section*, *Polytechnique Montreal*. His research interests focus upon evolutionary computational intelligence applied to engineering problems, such as condition monitoring. Furthermore, he works in the field of mechatronics design, and understanding and modeling activities of new product development processes for decision support purposes.